Generation and Conversion of Transverse Electromagnetic Modes

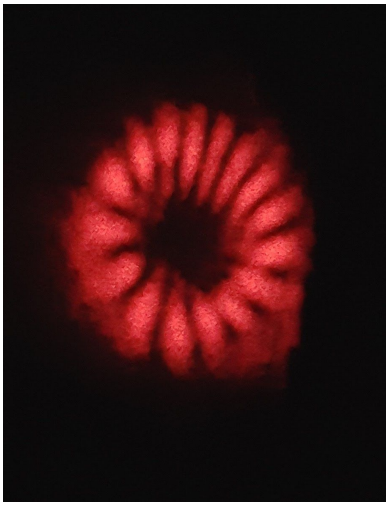

Max Stanley

Jay Rutledge and Marcus Lo

Laser Teaching Center

Department of Physics and Astronomy

Stony Brook University

Background

The conception of this project initially stemmed from interesting ideas surrounding the possible overlap between the quantum harmonic oscillator (QHO), and the nature of a resonant optical cavity. Quantum mechanics is based on the Schrodinger equation, and its solutions for the QHO are a discrete family that includes the Hermite Polynomials. These are special functions that are ubiquitous in physics. As an example, the same Hermite Polynomials form discrete solutions, in Cartesian coordinates, to the paraxial wave equation (an approximation we shall of course make), which describes the propagation of light in free space.

Our exploration of Hermite-Gaussian (HG) transverse electromagnetic modes (TEM) that are based on Hermite Polynomials led to an interest in another basis set, the Laguerre-Gaussian (LG) modes, which feature a circular symmetry rather than the rectangular symmetry of HG modes. Successful astigmatic mode conversion led us to various experiments focused on these unusual, orbital momentum carrying light beams. These experiments included a pursuit of the sinusoidal variant of these LG modes, which are of great interest to researchers at the Laser Interferometer Gravitational-Wave Observatory (LIGO).

Introduction

A **laser mode** is a laser-produced electromagnetic field which features a constant transverse distribution of intensity as it propagates. It can of course diverge or even lose power through attenuation while maintaining its particular “mode” designation. The most familiar mode (from the standard laser pointer) is the TEM_{00}, which is likely the only mode ever to be seen by those outside of the laser field (fig 1).

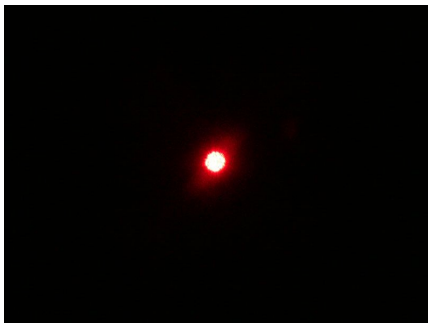

Figure 1: TEM_{00} mode has a Gaussian intensity distribution

Infinitely many more modes exist, however! These higher-order modes consist of an increasing number of both bright nodes and dark spaces in between them. There also exist **multi-modes** which aren't modes themselves, but rather conglomerations of actual modes. They often appear to be amorphous blobs, since they are simply linear combinations of real modes, elements of the basis set. These multi-modes, due to variations in Gouy phase (discussed later) between their differently ordered constituent modes, do not maintain their transverse intensity distributions throughout propagation.

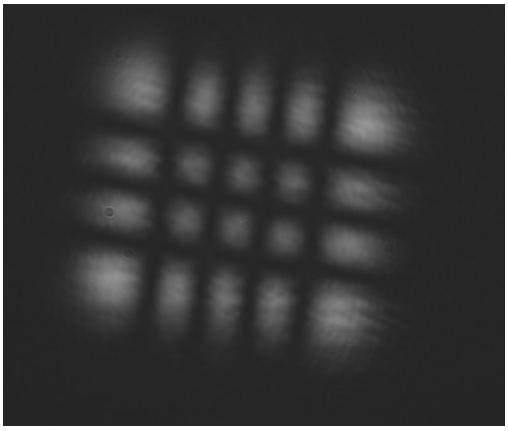

Figure 2: High order HG mode **(**TEM_{43} or HG_4^3)

The Hermite-Gaussian modes are an independent basis set of solutions to the paraxial wave equation, so they can be physically and mathematically converted to another independent set. Using an **astigmatic mode converter** (M.W. Beijersbergen), we converted the generated HG modes into their LG mode counterparts, which are solutions in cylindrical, rather than rectangular, coordinates.

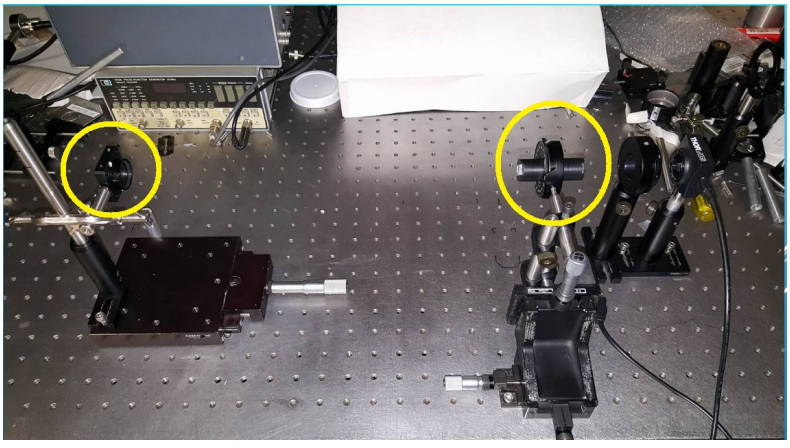

Figure 3: Mode matching lens (left) and astigmatic mode converter, respectively.

The Laguerre-Gaussian modes, unlike most other beams, carry not only **spin angular momentum** in the form of polarization, but **orbital angular momentum (OAM)** as well. OAM is caused by the field's spatial distribution, and can easily be understood by examining the wavefront of these LG beams, which are helical in nature.

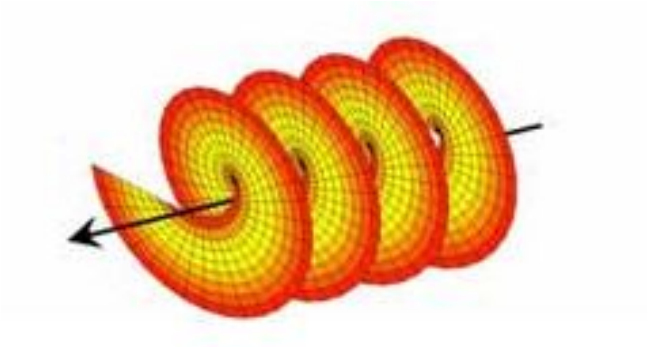

Figure 4: Helical wavefront carrying OAM

These LG beams have an inherent, "handedness," essentially the direction in which one would observe the azimuthal flow of energy in any given transverse plane of the beam. Due to phase and intensity relationships, it is possible to overlap two oppositely handed helical LG beams to form a new independent basis set, the sinusoidal Laguerre-Gaussian beams. These modes are notable due to their azimuthal, sinusoidal distribution of intensity and the extinction of any handedness i.e. no OAM.

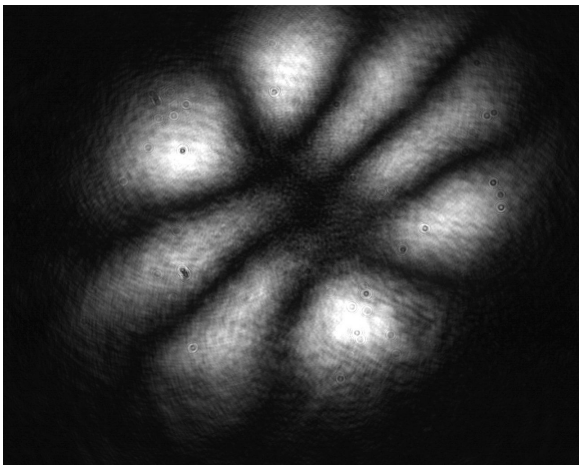

Figure 5: Sinusoidal LG_4^0 featuring a characteristic petal pattern

The generation of these three independent sets of modes and a variety of experiments showcasing their natures are outlined in this report.

Hermite-Gaussian Mode Generation

It was a consequence of the design of our laser that led to the generation of HG modes. An intracavity window at Brewster's angle destroyed the circular symmetry of the cavity. The Brewster window allows maximum transmission at one linear polarization, thereby polarizing the laser light. This inherent polarization proved to be helpful in the imaging procedure for these modes due to their ease of attenuation with an analyzer.

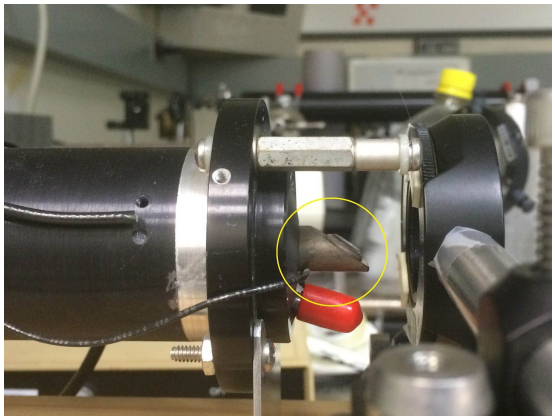

Figure 6: Brewster window at the end of the tube containing the gain medium (HeNe)

The generation of variously ordered HG modes began with the manipulation of a 50 micrometer diameter wire inside the cavity of an open-cavity, 632.8 nm HeNe laser. The laser had a fixed, high reflectance, 60cm radius of curvature spherical concave mirror behind the gain medium, and a linearly translatable output coupler (OC) mirror of matching curvature but with a few percent transmission. Fixed to a track, the OC mirror could be moved between positions 35 cm to 60 cm from the HR mirror. The latter position results in a confocal cavity. Spatially higher-order modes are large compared to the simple TEM_{00} mode, and their resonant conditions in the cavity required components traveling at larger angles. In an effort to achieve the highest order modes possible, we moved the OC mirror as close to the HR mirror as we could in order to better support these large angles. Within the cavity, we mounted an adjustable iris which could be used to obstruct the higher angles if specific, lower-order modes were desired. In practice, we found that the easiest way to generate different higher order modes was to place a hair or very thin wire across the iris, in the path of the beam. This allows oscillation in the cavity, only for modes possessing null where the hair or wire falls.

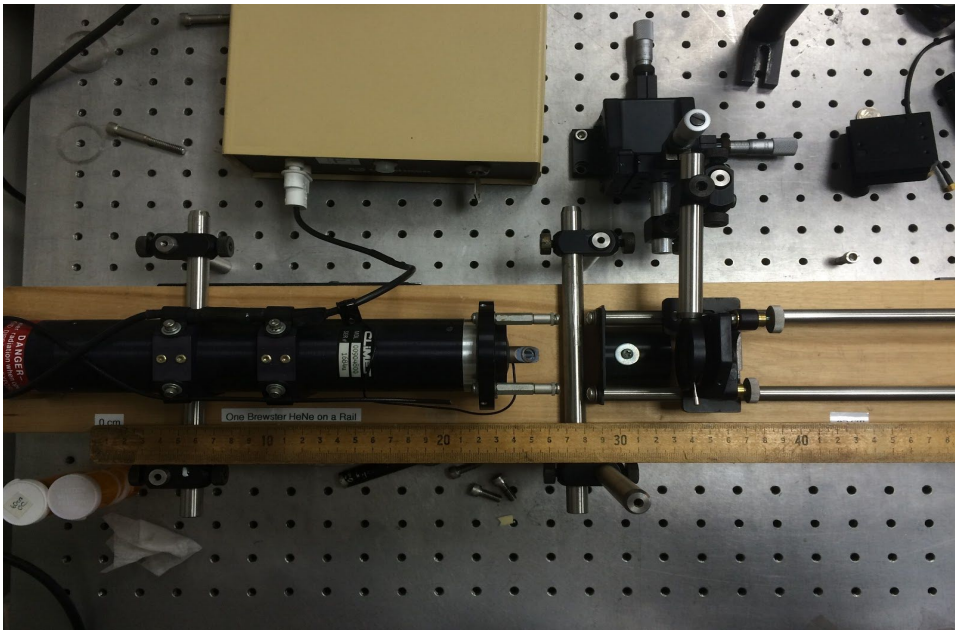

Figure 7: Open-cavity laser setup with iris mounted intracavity directly in front of OC mirror

We then tuned the OC mirror to achieve as large a multimode as possible and then swept the hair through the beam, observing the surviving modes which were often of high order.

A wide array of HG modes were achieved, and their images were captured using a simple Thorlabs CCD camera.

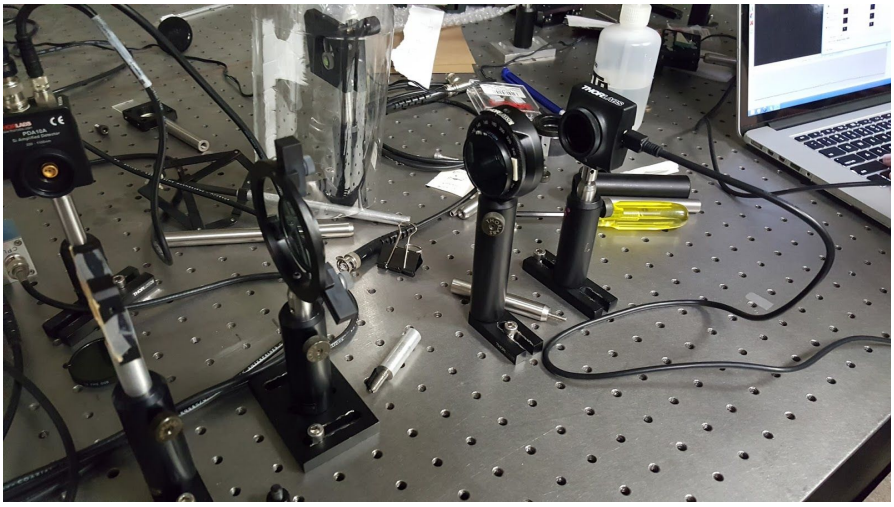

Figure 8: The light was attenuated using a single linear polarizer in a rotating mount.

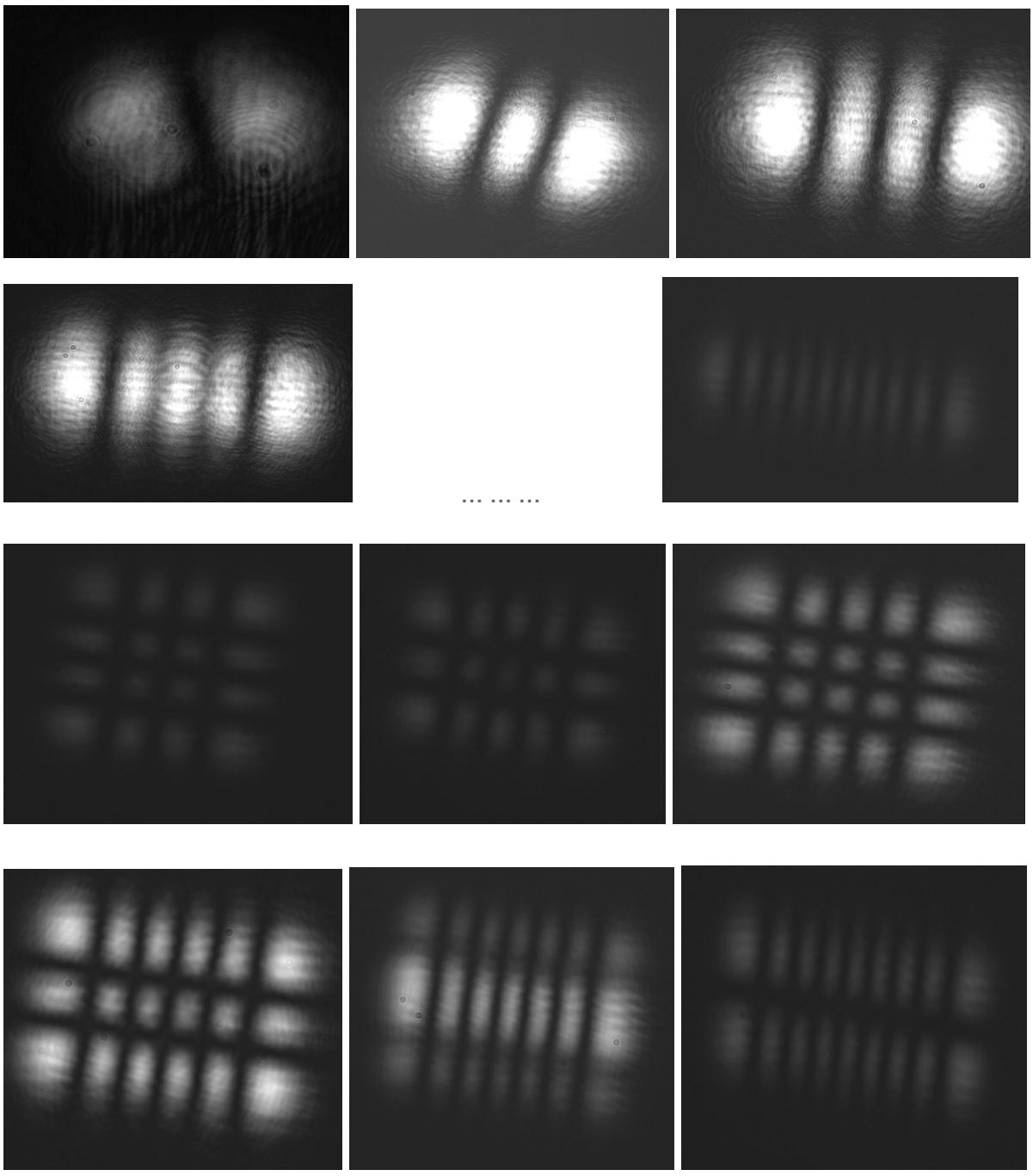

Figure 9

Rows 1 & 2: HG_0^1 , HG_0^2 , HG_0^3, HG_0^4, and up to HG_0^9

Rows 3 & 4: Arbitrary high order modes: HG_3^3 , HG_4^2 , HG_4^3 , HG_5^2 , HG_6^2, HG_8^1

Conversion of Hermite-Gaussian Modes to Laguerre-Gaussian Modes

The conversion from HG to LG modes was performed with an astigmatic mode converter, or AMC (M.W. Beijersbergen). The AMC consists of two cylindrical lenses of equal focal lengths, separated by a distance of $\sqrt{2}f$.

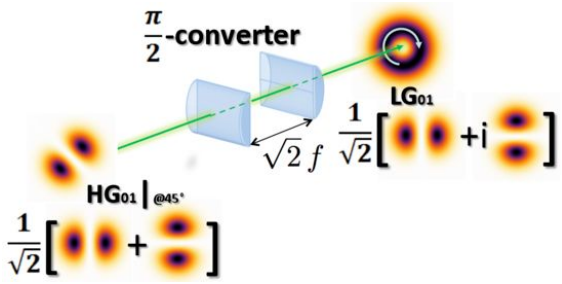

Figure 8: Conversion of an HG mode

Any Hermite-Gaussian mode passing through the astigmatic mode converter is transformed into a Laguerre-Gaussian mode with $l = |m - n|$, and $p = min(n,m)$. Due to interaction of the input beam in only one dimension, the Gouy phase can be exploited (with proper mode matching). A 45° linearly polarized HG mode, separated into the two transverse intensity planes in (x,z) and (y,z), accumulates different Gouy phases while passing through the waist within the cylindrical lenses.

Gouy Phase

The Gouy phase is a phase accumulated throughout the propagation of a Gaussian beam. As light moves through the beam waist, the distance between wavefronts is slightly increased, and continuity necessitates an increase in local phase velocity. The particular converter we used adds a phase of $\pi/2$. The accumulated Gouy phase is given by the equation:

$$\phi_G(z) = arctan(\frac{z}{z_R})$$

Mode Matching

The input beam must be matched to the conditions required by the converter. Gaussian optics plays a critical role in properly positioning the beam for the correct manipulation of the Gouy phase. Mode conversion is achieved when the beam waist is placed at the center of the converter barrel, directly between the two cylindrical lenses. To do this, a single spherical lens is placed at a particular location dictated by the waist position and Rayleigh range of the laser.

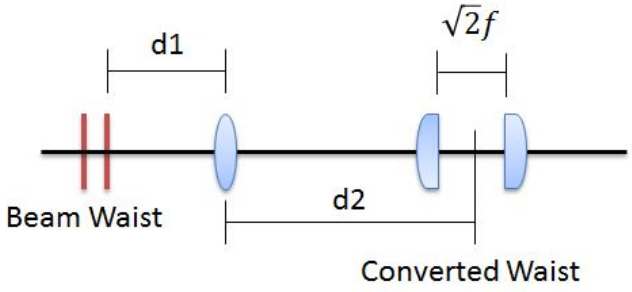

Figure 10: Relative positions of beam waists and lenses

Since the laser cavity was concentric, we determined the position of the waist to be exactly between the HR and OC mirrors. We profiled the beam at a distance much larger than the expected Rayleigh range of the beam away from its waist. This allowed us to determine both the waist size and the actual Rayleigh range. The full angle divergence can be approximated as:

$$\Theta \approx \frac{2\lambda}{\pi w_0}$$

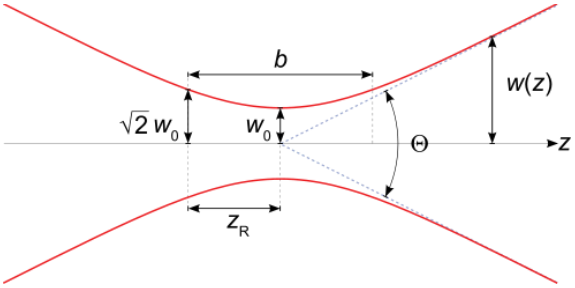

The Rayleigh range was calculated using the relationship derived from basic Gaussian optics:

$$z_{\mathrm{R}} = \frac{\pi w_0^2}{\lambda}$$

The distances d_1 and d_2 are calculated with the intent that the Rayleigh range of the beam incident on the mode converter will be:

$$z_0' = (1 + 1/\sqrt{2})f$$

Two intermediate parameters are calculated:

$$M_r = \left|\frac{f}{d_1 - f}\right| \qquad\qquad r = \frac{z_0}{d_1 - f}$$

In order to solve for the magnification:

$$M = \frac{M_r}{\sqrt{1 + r^2}}$$

Which directly relates the original and transferred Rayleigh ranges:

$$z_0' = M^2 z_0$$

The distance from the mode matching lens to the waist positioned at the center of the mode converter is related to d_1 and M by:

$$(d_2 - f) = M^2(d_1 - f)$$

The focal length of the mode matching lens can be selected somewhat arbitrarily, so long as it's placed at the correct distance from the laser beam waist.

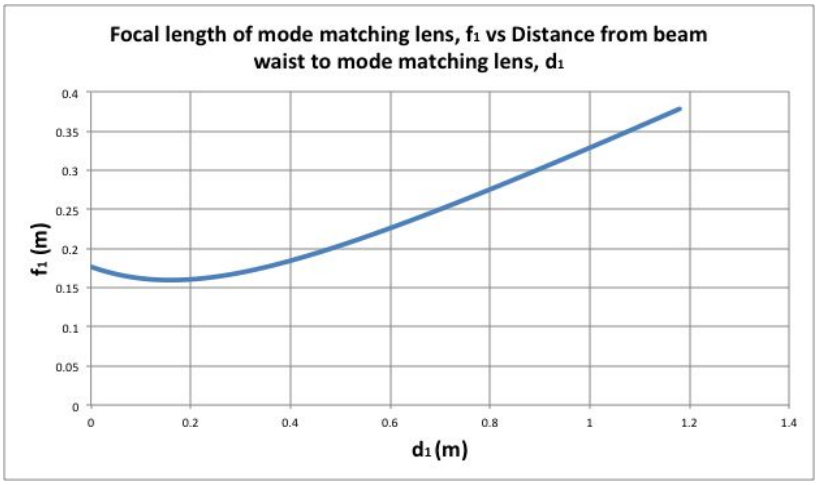

Figure 11: Mode matching lens positioning graph

In practice, the positions of both the mode matching lens and the mode converter are more tolerant than the numerous equations imply, and converted modes can be observed over a range of several centimeters for each. We converted and imaged a variety of modes. Again, the index conversion from Hermite-Gaussian m's and n's to the Laguerre-Gaussian p's (radial) and l's (azimuthal) goes as follows:

$$l = |m - n|, \quad p = min(n,m)$$

Mathematically, Hermite and Laguerre Gaussians are simply the products of Hermite and Laguerre associated polynomials, respectively, with Gaussian functions. The indices clearly change in the transformation, as well as the associated polynomials.

$$E_{nm}(x,y,z) = E_0 \frac{w_0}{w(z)} \cdot H_n\left(\sqrt{2}\frac{x}{w(z)}\right)\exp\left(-\frac{x^2}{w(z)^2}\right) \cdot H_m\left(\sqrt{2}\frac{y}{w(z)}\right)\exp\left(-\frac{y^2}{w(z)^2}\right) \cdot \exp\left(-i\left[kz - (1+n+m)\arctan\frac{z}{z_R} + \frac{k\left(x^2+y^2\right)}{2R(z)}\right]\right)$$

Hermite-Gaussians

$$u_{p,l}^{\mathrm{hel}}(r,\phi,z) = \frac{1}{w(z)}\sqrt{\frac{2p!}{\pi(|l|+p)!}}\quad e^{\mathrm{i}\,(2p+|l|+1)\Psi(z)} \times \left(\frac{\sqrt{2}r}{w(z)}\right)^{|l|} L_p^{(|l|)}\left(\frac{2r^2}{w(z)^2}\right) e^{-\mathrm{i}k\frac{r^2}{2q(z)}+\mathrm{i}l\phi}$$

Laguerre-Gaussians

Here, H_n and L_p are the Hermite and Laguerre polynomials. E_0 is the electric field amplitude, k is the wave vector, and $w(z)$ gives the beam waist at position z.

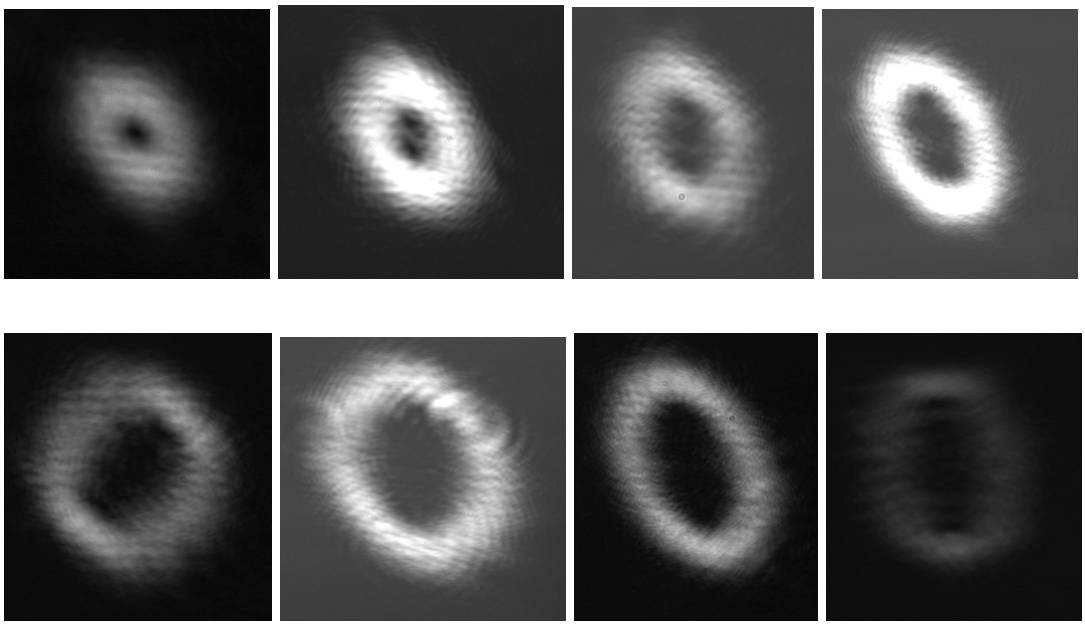

Figure 12

Rows 1 & 2: LG_1^0 through LG_8^0 (increased ring diameter and decreased ring thickness)

Higher order LG modes acquire more rings, according to the index *p*, while the higher order *l* index is responsible for increased ring diameter.

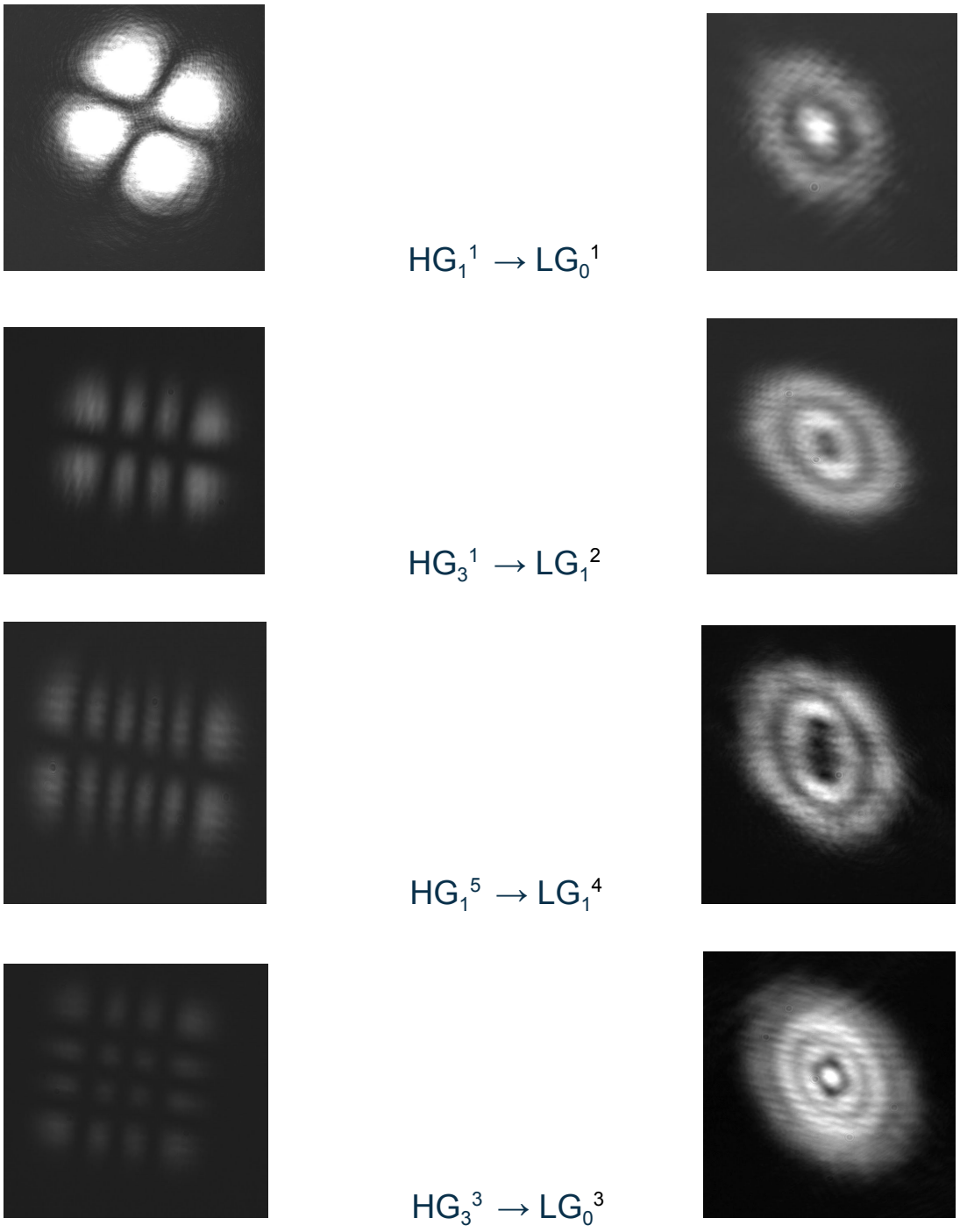

Figure 13: LG modes with their corresponding HG mode

One notable characteristic of the LG modes we generated is their ellipticity. Variation in the position of the mode matching lens, as well as rotation of the mode converter altered

the degree of ellipticity; however, we often couldn't manage to perfectly circularize the modes. Careful alignment of the optics, especially meticulous placement of the beam through the center of the mode converter, allowed for greater circular quality modes, but in the end, they were still slightly elliptical.

Generation of Sinusoidal Laguerre-Gaussian Modes

Sinusoidal Laguerre-Gaussian modes, like the Hermite-Gaussians and helical Laguerre-Gaussians, are an independent set of solutions of the paraxial wave equation. A combination of oppositely-handed helical Laguerre-Gaussian modes eliminates the orbital angular momentum and results in a sinusoidal distribution of intensity azimuthally.

$$u_{p,l}^{\mathrm{hel}}(r,\phi,z) = \frac{1}{w(z)}\sqrt{\frac{2p!}{\pi(|l|+p)!}}\; e^{\mathrm{i}\,(2p+|l|+1)\Psi(z)} \times \left(\frac{\sqrt{2}r}{w(z)}\right)^{|l|} L_p^{(|l|)}\left(\frac{2r^2}{w(z)^2}\right) e^{-\mathrm{i}k\frac{r^2}{2q(z)}+\mathrm{i}l\phi}$$

$$\Rightarrow \quad u_{p,l}^{\mathrm{cosine}}(r,\phi,z) = \frac{2}{w(z)}\sqrt{\frac{2p!}{\pi(|l|+p)!}}\exp\left(\mathrm{i}\,(2p+|l|+1)\,\Psi(z)\right) \times \left(\frac{\sqrt{2}r}{w(z)}\right)^{|l|} L_p^{l}\left(\frac{2r^2}{w(z)^2}\right)\exp\left(-\mathrm{i}k\frac{r^2}{2q(z)}\right)\cos(l\phi)$$

$$\cos x = \mathrm{Re}\{e^{ix}\} = \frac{e^{ix}+e^{-ix}}{2}$$

Addition of two helical LGs yields a sinusoidal LG using the exponential trigonometric identity

The handedness of a helical LG mode will switch upon a single reflection (or a cumulative odd number of reflections). We used a Dove prism, which inverts an image through a single instance of total internal reflection, to achieve this flip of handedness.

Our setup to overlap two identical, but oppositely handed, helical LG modes was a Mach-Zehnder interferometer. After a beam splitter, one arm contained the Dove prism and the other transported the original helical LG mode. A beam splitter recombined the two, now opposite handed, modes.

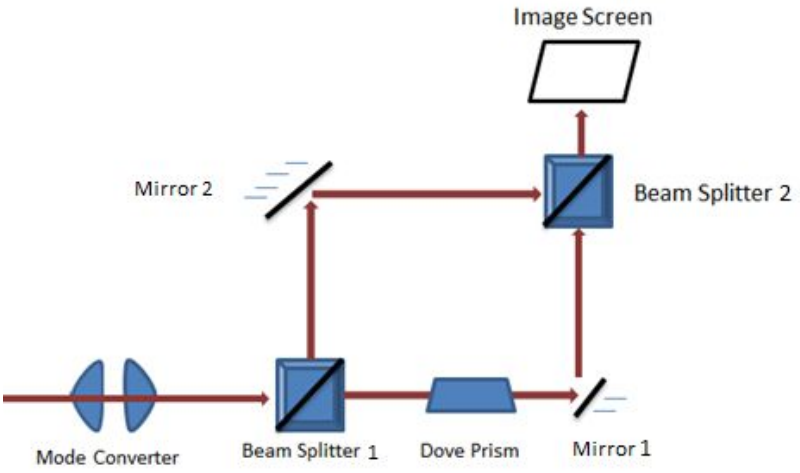

Figure 14: Mach-Zehnder interferometer accepting a single helical LG mode

By overlapping the two modes exiting the Mach-Zehnder in the near field using mirror 1, and then overlapping them in the far field by adjusting beam splitter 2, we successfully interfered the modes in a manner similar to walking the beam.

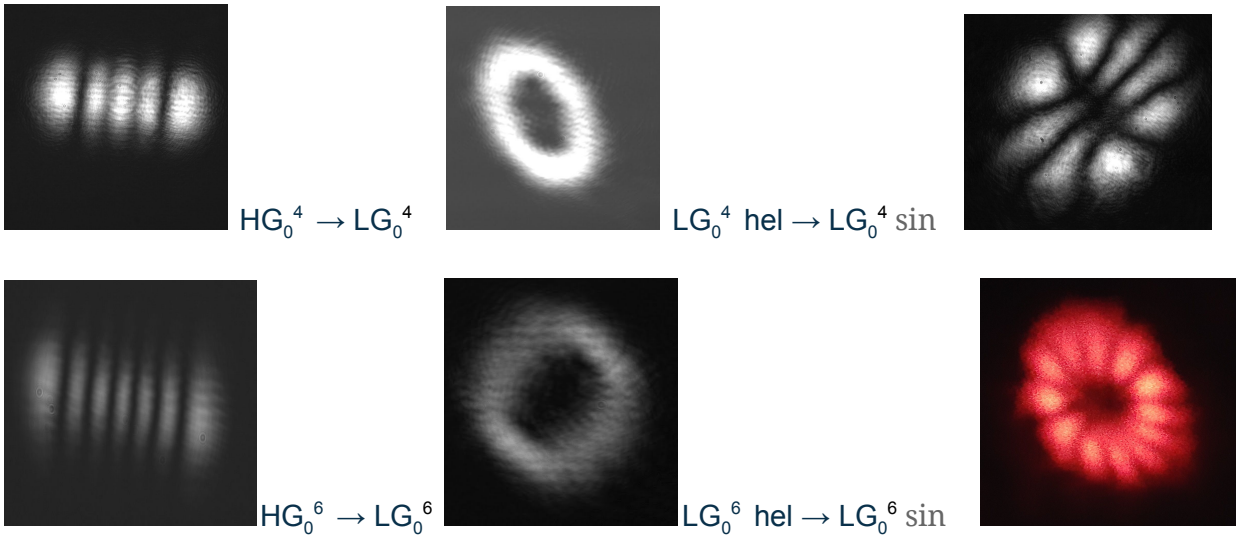

Figure 14: HG to sinusoidal LG mode conversion. The number of petals is twice the *l* index of the helical LG mode (superposition of two modes).

Fork Pattern and Optical Vortices

Probably due to the ellipticity of our input LG helical modes, we were unable to

resolve interference patterns beyond the **fork pattern** for modes with *p* indices greater than 0.

The fork pattern arises from the interference between two oppositely handed helical LG modes or a single helical LG and a reference plane wave. A phase discontinuity at the dark center of the fork is an optical vortex, a region in which the phase is undefined. The number of prongs in the fork pattern indicates the topological charge *l* (the integer multiple of ħ in determining the angular momentum) in the case of the single helical LG mode. The combined modes would generate a fork pattern with twice as many prongs as the topological charge of the individual constituent modes.

Only a complete overlapping of the two helical LG modes will yield a sinusoidal LG mode. The fork pattern is the result of off-center overlap. When fine tuning the interferometer, moving one of the modes towards the “handle” of the fork seems to give positive results.

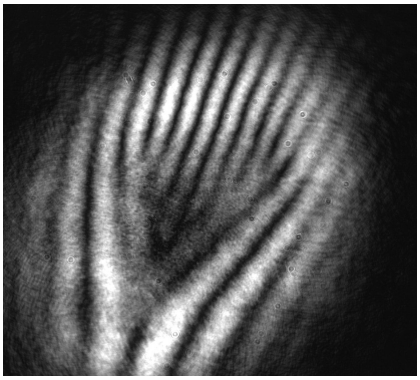

Figure 15: Fork pattern from two LG_0^5 helical modes.

Phase Analysis of Laguerre-Gaussian Modes

To conduct a phase analysis of helical and sinusoidal LG modes, we constructed a dual Mach-Zehnder system that provided a reference plane wave from an expanded HG lobe. Essentially, the setup from figure 14 was placed entirely within one arm of a larger Mach-Zehnder interferometer.

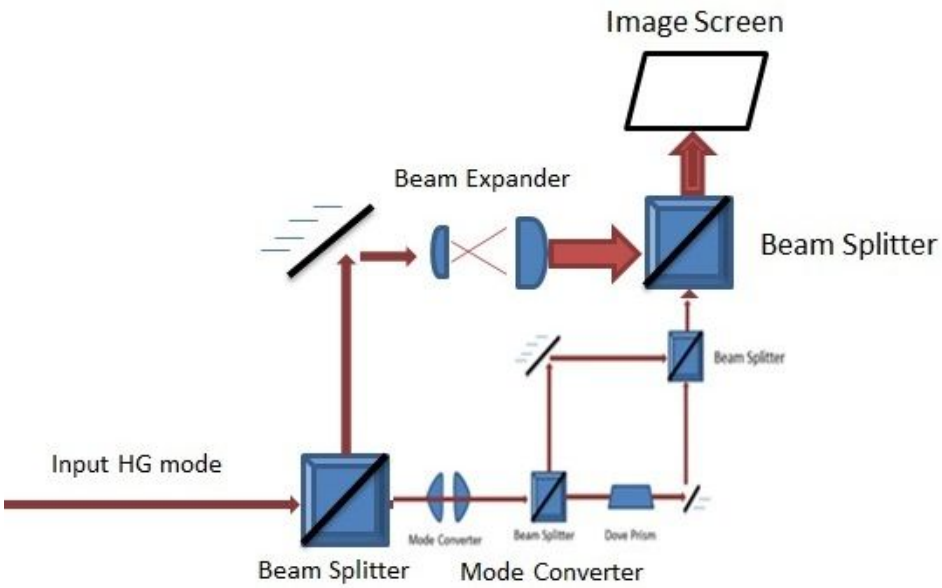

Figure 16: The “Mach 2” Interferometer

By blocking either arm of the inner interferometer, a phase analysis of either handed helical LG mode could be performed. Without blockage, a sinusoidal LG mode is interfered with the reference plane wave. Fine tuning of this system was tedious in the case of sinusoidal mode interference because the mode could not be readily positioned. Since it consisted of two helical modes, each had to be meticulously adjusted each time to reform the sinusoidal mode in its new position. Fortunately, the HG lobes were expanded enough where repositioning of the sinusoidal LG mode was not necessary for the most part.

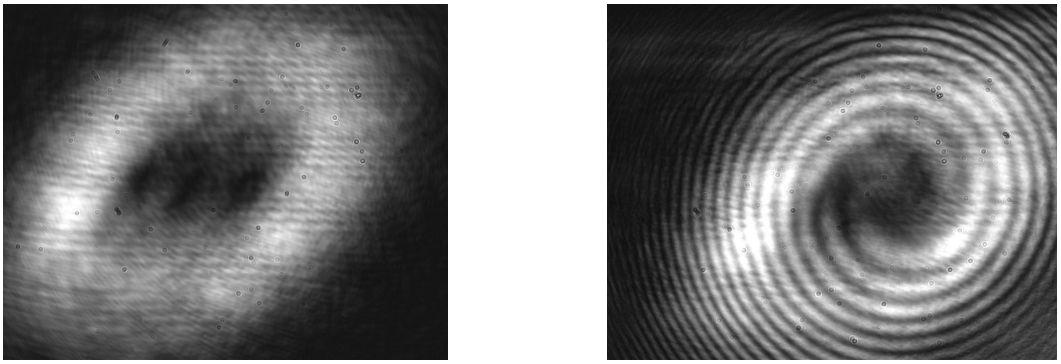

Figure 16: Interference of a single helical LG mode with a reference plane wave. The Dove prism interferometer path is blocked and the number of spirals in the interference pattern corresponds to the index of the input mode (LG_0^3 yields 3 spirals). The spirals move in a clockwise fashion.

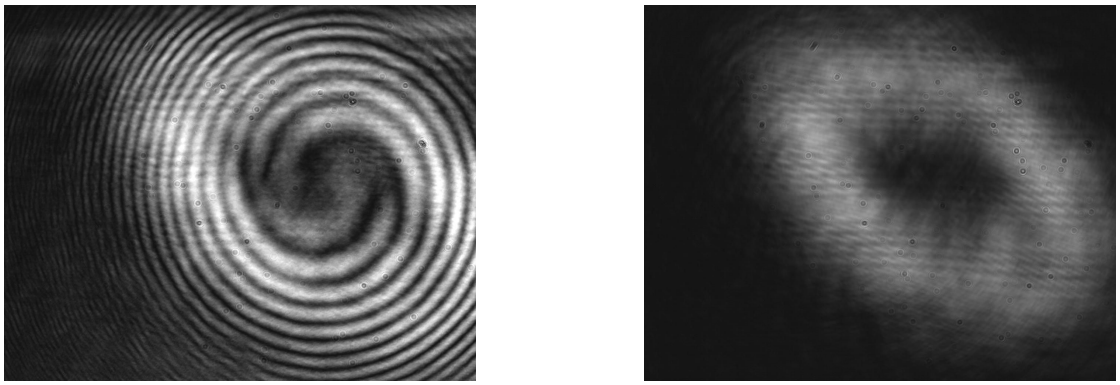

Figure 17: Interference of a single helical LG mode, oppositely handed from that used in figure 16. The path without the Dove prism is blocked and the spirals move in a counterclockwise fashion.

Interference of a sinusoidal LG mode resulted in a striated petal pattern. A sinusoidal LG_0^3 mode shows an offset in the first three interference rings, demonstrating the correlation between mode number and resultant pattern. The sinusoidal intensity distribution remains obvious in the interference pattern.

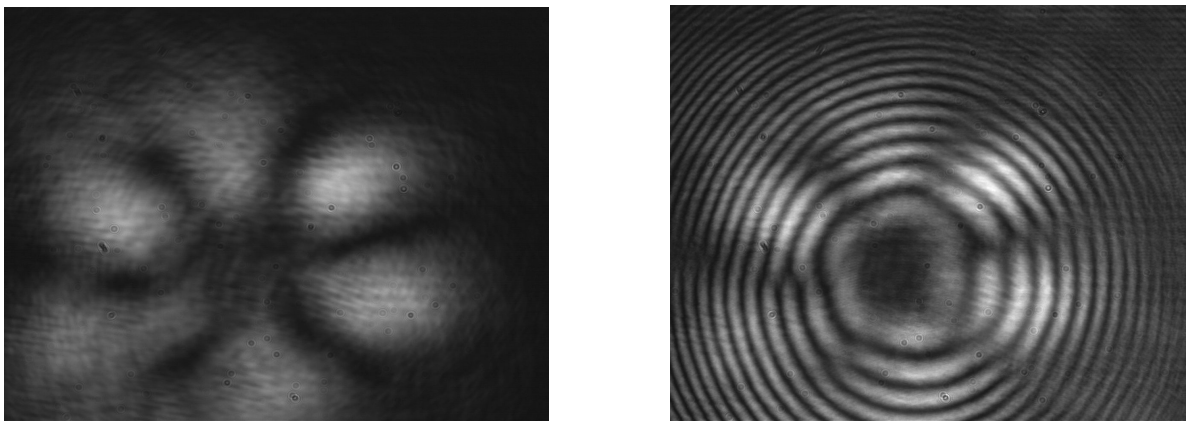

Figure 18: Sinusoidal LG_0^3 interference with a reference HG lobe.

Additional Experiments

We carried out additional experiments on LG modes with orbital angular momentum.

Azimuthal Energy Flow

Due to OAM, the cutting of a helical LG mode with a straight edge will allow observation of its azimuthal flow of energy, as shown by Arlt. Like planetary orbits, the inner rings of a high p order LG mode will rotate faster than the outer rings.

Figure 19: Cut mode imaged at 10 cm and 14 cm from the straight edge.

Figure 19 shows a counterclockwise flow of energy across a span of 4 cm.

Double-slit Diffraction

Sending a helical LG mode through a double slit results in an offset in the fringe pattern due to a phase gradient across the wavefront. The evenly spaced and parallel fringes seen in the conventional pattern obtain a slant that places them in line with the fringe l spaces over (right or left depending on handedness of the mode).

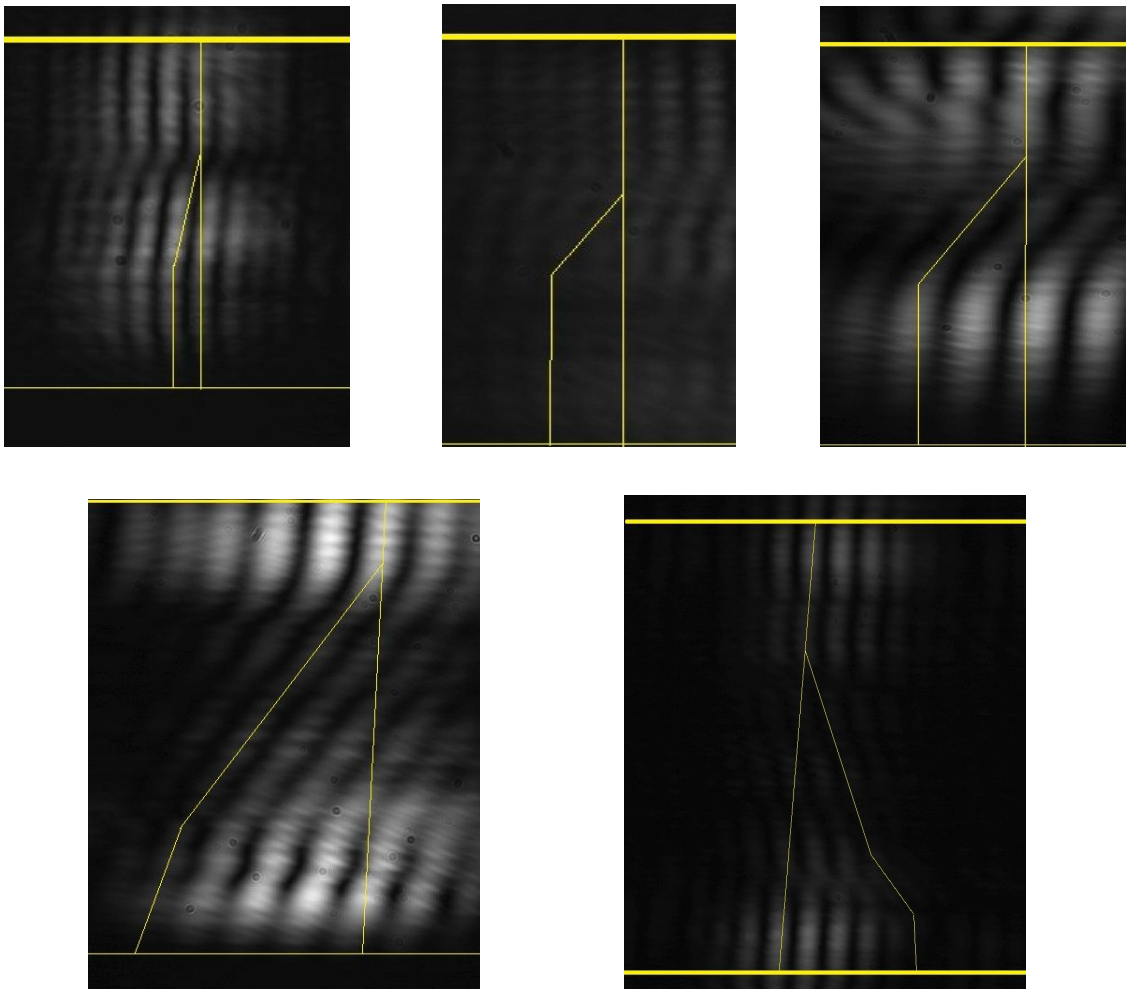

Figure 20: Double slit diffraction pattern for LG_0^1 through LG_0^5 with reference lines drawn. The effect is not as apparent on LG_0^3 due to some blending of the fringes.

Conclusion

High order Hermite-Gaussian modes were generated through manipulation of an open-cavity HeNe laser, the use of an astigmatic mode converter. Then, with the use of an astigmatic mode converter, and a dual Mach-Zehnder interferometer, we generated Laguerre Gauss modes, both helical and sinusoidal. The creation of clear, high order HG modes, took a great deal of time with manipulation of cavity conditions and the alignment of optics. While these experiments were largely qualitative, future work may involve simulation and quantitative phase analysis in MATLAB. We are especially interested in comparing the interference pattern of the sinusoidal LG mode (Fig. 18) with the theoretically predicted pattern.

References

[1] L. Allen, M. W. Beijersbergen, R. J. C. Spreeuw, and J. P. Woerdman, Orbital angular momentum of light and the transformation of Laguerre-Gaussian laser modes, Phys. Rev. A 45, 8185

[2] J. Courtial, M.J. Padgett, Performance of a cylindrical lens mode converter for producing Laguerre–Gaussian laser modes, Optics Communications 159(1):13-18 · December 1998

[3] Astigmatic laser mode converters and transfer of orbital angular momentum; M.W. Beijersbergen, L. Allen, H.E.L.O van der Veen and J.P. Woerdman, 1992

[4] Creating optical vortex modes with a single cylinder lens, *Hamsa Sridhar, Martin G. Cohen and John W. Noe, Laser Teaching Center, Stony Brook University*, SPIE 7613, Complex Light and Optical Forces IV, 76130X

[5] *An experiment to observe the intensity and phase structure of Laguerre-Gaussian laser modes* by M. Padgett, J. Arlt, and N. Simpson (*American Journal of Physics, Jan. 1996)*

[6] J. Arlt, Handedness and azimuthal energy flow of optical vortex beams, Journal of Modern Optics Volume 50, Issue 10, 2003